Journal of Sciences, Islamic Republic of Iran 17(2): 127-145 (2006) http://jsciences.ut.ac.ir
University of Tehran, ISSN 1016-1104

Major, Trace and REE geochemistry of Paleo-Tethys Collision-Related Granitoids from Mashhad, Iran

M.H. Karimpour,[1,*] L. Farmer,[2] C. Ashouri,[1] and S. Saadat[3]

[1]*Department of Geology, Faculty of Sciences, Ferdowsi University of Mashhad, Mashhad, Islamic Republic of Iran*
[2]*Department of Geological Sciences, University of Colorado, 399UCB, Boulder, CO 80309, USA*
[3]*Department of Geology, Azad Islamic University of Mashhad, Mashhad, Islamic Republic of Iran*

Abstract

The study area is located in northeastern Iran (south of Mashhad). The Paleo-Tethys remnants (meta-ophiolite and meta-flysch) were intruded at three different episodes of magmatism (Triassic to Cretaceous time). 1) Dehnow-Kuhsangi hornblende biotite tonalite-granodiorite; 2) Sangbast Feldspar monzogranite; and 3) Khajehmourad biotite-muscovite leucogranite and pegmatite. They are moderately peraluminous to highly felsic peraluminous S-type granitoid. Paleo-Tethys opened in Silurian time and subduction under Turan plate was started in Late Devonian. By Late Carnian (225 m.y. ago) there was no Paleotethys left on an Iranian transect. Turan plate is abducted over Iran Plate. Only two stages of low grade regional metamorphism are exposed, Hercynian orogeny (Late Paleozoic) and Cimmerian orogeny (Jurassic time). Ophiolites constitute allochthonous sheets and they are dated by 40Ar-39Ar, 281.4 and 277.4 Ma. Dehnow to Kuhsangi tonalite-granodiorite (Early Triassic) are meta to moderately peraluminous S to I-type granitoids. They are sub-alkaline, calcic-type. They have low values of magnetic susceptibility [(1.5 to 2.5) × 10^{-5} SI]. Sangbast feldspar monzogranite porphyry (Late Triassic) is moderately peraluminous, K-rich calc-alkaline type. Biotite-muscovite leucogranite and late pegmatite dikes (Jurassic age) are highly felsic peraluminous S-type granitoids. They are syn-collision granite. They have low values of magnetic susceptibility [(0.1 to 0.6) × 10^{-5} SI]. Total REE content of tonalite-granodiorite is 101-136, in feldspar monzogranite is 221-238 and in leucogranite is 130-170 ppm. The leucogranite has the highest [(La/Yb)N = 37-124] tonalite-granodiorite has the lowest [(La/Yb)N = 7 to 22]. The Eu anomalies (Eu/Eu* = 0.55 to 1.1) is low in all of them. Tonalite-granodiorite magma has originated from a mafic source. Feldspar monzogranite has originated from a deeper source and contaminated in the crust. Biotite-muscovite leucogranite may have originated from the crustal materials.

Keywords: Mashhad; Paleo-Tethys; Granite; Dehnow; Vakilabad

1. Introduction

The study area is located in northeastern Iran and lies between Longitude 59° 15′ E to 59° 45′ E and Latitude 36° N to 36° 30′ (Fig. 1a). The Binaloud Mountains are part of Paleo-Tethys remnants (meta-ophiolites and meta-flysch) which were intruded by tonalite, granodiorite, feldspar maozogranite, biotite-muscovite leucogranite and pegmatite dikes at different episodes (Triassic to Cretaceous times).

The Binaloud Mountains are situated south and west of Mashhad city. The southern and western part of

[*]*E-mail: mhkarimpour@yahoo.com*

Mashhad city lies on the remnants of the Paleo-Tethys and the younger intrusive rocks (Fig. 1a).

Previous works: Jarchovski *et al.*, [1] did some mineral reconnaissance on granite, tonalite, ophiolite and metamorphosed rocks in Binaloud region. The earliest petrographic studies on Mashhad granites were carried out by Albertie & Moazez [2]. K-Ar ages of muscovite and biotite (4 samples) from two locations within the main granite body gave the following ages: 145, 120, 135 and 146 (±3) m.y., Late Jurassic Early Cretaceous) [3]. Pebbles and cobbles of tonalite, granodiorite and feldspar monzogranite are found within the conglomerates of Early Jurassic. This indicates that the intrusive rocks were intruded at different times. Plimer & Moazez [4] studied the petrography of Dehnow tonalite and its xenocryst garnets. Majidi [5] did his Ph.D. thesis on the ophiolites, metamorphic rocks and granitic rocks. Alavi [6-8] studied the structural characteristics of the area in some details. Valizadeh & Karimpour [9] and Karimpour *et al.* [10] studied the petrography, major element geochemistry and metallogeny of the granitoids. Mirnejad, [11] did his M.Sc. thesis on the petrography and major element geochemistry of intrusive rocks. Iranmanesh & Sethna [12] did a general study on Mashhad granites. Abbasi [13] did his M.Sc. project on both regional and contact metamorphic rocks. Ghazi1 *et al.*, [14] studied the geochemistry, and determined the age of, the Mashhad Ophiolite.

The purpose of this study is to find out the petrochemistry, paleotectonic setting, and petrogenesis of Mashhad granitoids.

2. Geological Setting

During Paleozoic, Iran and Arabian plates formed a coherent terrain and were separated from the Turan Plate by the Paleo-Tethys. Stampfli, [15-17]; and Stampfli & Pillevuit [18,19], presented evidence from Alborz and elsewhere that the Paleo-Tethys opened in Silurian time. In the Late Paleozoic, or Early Triassic, the Iran Plate drifted away from Arabia plate by the opening of the Neo-Tethys and Iranian Plate collided with the Turan Plate. In Iran, Turkey, and Greece the closure of Paleo-Tethys did not take place before Carnian (late Triassic, 231 m.y. ago). By the late Carnian (about 225 m.y. ago) there was no Paleotethys left on an Iranian transect [15,17-20].

The Binaloud range in northeastern Iran, south of Mashhad, is a remnant of Paleo-Tethys. To the west, it extends to Alborz Mountains, Azerbaijan, Armenia, Turkey and Eastern Europe. To the east, it extends to Hindu-Kush Mountains, north of Afghanistan and India. The obduction of the Paleo-Tethys remnants and their emplacement over the Iranian continental margin must have occurred Pre-Late Triassic [15,17-20] It is concluded by Alavi [8] and Stockline [21], that the initiation of the Iranian microcontinent-Turan collisional processes had also started prior to the end of Triassic.

Aghdarband tectonic window, east of Mashhad, provides information concerning Per-Triassic and Triassic rocks formed along the Turan Plate. Permo-Triassic rocks of Aghdarband are the basement of eastern Kopeh Dogh Range.

The Pre-Triassic rocks of Aghdarband are intensively faulted and trusted. A high grade marble is overlain by conglomerates, and a sequence of clastic rocks mainly consisting of coarse sandstone and fine-grained breccia with intercalations of slates (700 m thick). At the top of this sequence, there is a thin bedded dark grey to black limestone with black shale and dark green diabase. The conodont species *Palmatolepis triangularis* and *Palmatolepis minuta* found within the black limestone suggest a Late Devonian age [22].

The conglomerate at the base of this clastic series contains well rounded pebbles of the underlying bluish-grey marble. This gives evidence of a strong metamorphism which took place in pre-Late Devonian times [22].

The Triassic series in Aghdarband has 1200 to 1500 m thick, is subdivided into 3 formations [23]. The age was determined based on different types of fossils. The older formation is a shallow limestone (Early Triassic) and the second formation is a deep water andesitic to trachyitic volcanoclastic (middle early Late Triassic) and finally the third formation is mudstone, shale and siltstone (Late Triassic). A coal bearing horizon is present between marine and non-marine shales.

The epiclastic volcanic sediments originated from an active volcanic arc along the Turan plate. Subduction of Paleo-Tethys oceanic crust under Turan plate started in Late Devonian and continued into Triassic and led to the formation of a volcanic arc [23]. During Permo-Triassic, a marginal basin developed along the new Paleo-Tethyan active margin. This basin is regarded as a back arc or a continental rift [23]. In the back arc of Aghdarband area, volcanic activity started in Scythian and ceased in Late Norian. This type of volcanic-sedimentary rocks is reported in Band-i-Turkestan and other areas [23]. Based on exploration drilling data, the Paleozoic rocks of Turan plate are metamorphosed up to granulite in some areas [23].

Ruttner [22] identified three major orogenies in Aghdarband by 1) Pre-Cambrian or Caledonian, 2) Hercynian orogeny which caused a slight meta-

morphism in the Paleozoic rocks of Aghdarband, and 3) a strong Early Cimmerian orogeny which caused alpine-type structural features.

The abducted remnants of the Paleo-Tethys Ocean in Binaloud range, Iran, include several rock assemblages including ophiolite complexes, Meta-flysch and some submarine pyroclastics. They are being intruded by tonalite, granodiorite, feldspar monzogranite, and biotite-muscovite leucogranite.

Based on the geophysical studies carried out by Kunin *et al.*, [24], the thickness of the continental crust in Binaloud area is about 48 to 50 km.

Ophiolite complexes: Ophiolites are exposed mainly along the northern part of the study area (Fig. 1a). They can be divided into two complexes: 1) Nourabad and 2) Chehar-cheshmeh. The Nourabad complex (earlier known as Virani) is exposed along the road from Mashhad to Shandiz (about 25 km from Mashhad) around the village of Nourabad (Fig. 1a). The Chehar-cheshmeh ophiolite complex is exposed between Vakilabad and Khalaj (Fig. 1a). The southwestern part of Mashhad city is mainly built on this complex.

According to detailed studied by Alavi [7-9] "ophiolites constitute allochthonous sheets emplaced onto the surrounding flysch deposits by a low angle, pre-collisional ductile thrust system that is associated with mylonites and mesoscopic sheared-off fault-drag fold". These mylonites are few centimeters to a meter wide. Pre-obductional as well as syn-obductional deformations have produced complex structures in the Paleo-Tethys remnants [8]. Ophiolites and the surrounding meta-flysch were deformed by two phases of coaxial isoclinal folding with subhorizontal axes [9]. As a result, ophiolite and the meta-flysch appear as parallel narrow strips. Based on this appearance, Majidi [25] instead of ophiolite called them as ultrabasic flows.

Based on REE and tectonomagmatic classification diagrams, there are at least two different types of basalts [14]. Type-A basalts show volcanic arc-like chemical characteristics, whereas the type-B basalts have E-MORB-like chemical affinity. Type-A basalts have LREE enriched patterns [(La/Yb)ave = 6.7 and (La/Sm)ave = 3.4] in comparison to the type-B (E-MORB-like) basalts with [(La/Yb)ave = 2.3 and (La/Sm)ave = 1.05. Tow hornblende gabbros were dated by 40Ar-39Ar (281.4 Ma and 277.4 Ma) corresponding to isochrone ages of 287.6 and 281.7 Ma. In a separate K/Ar analysis, the same two samples gave values of 273 and 265 Ma, suggesting Late Pennsylvanian-Early Permian ages, such as Paleo-Tethys age for the oceanic crust [14].

The ophiolites are effected by different episodes of regional metamorphism. In areas near to thrust zone, they are strongly sheared. In areas near to granitoid intrusive rocks, amphibolites are formed (Khalaj and some other areas).

Nourabad complex includes mainly peridotite, with minor pyroxenites and some gabbros. Peridotites are mainly wehrlites and some lherzolites. These rocks are affected by low-grade regional metamorphism and they are mainly serpentinized. Due to intensive thrusting and folding, they developed strong shearing in some zones. Clinopyroxenes form large crystals and poikilitic textures. Olivine pseudomorphs are mainly found as small rounded crystals, and plagioclase is rare or absent. In dunitic rocks, olivine is subhedral. Gabbros are founded in several areas, they are medium to fine grained and they don't show any layering.

The Chehar-Cheshmeh and Reza Shar ophiolite complexes are much larger. Pillow basalts, cherts and pelagic sediments are more abundant in this area. Pillow lavas are found in Chehar-Cheshmeh and nearby areas. Serpentinite is being mined for making special pots (slow cooking) and different handicrafts.

Meta-flysch: The meta-sediments are slates, quartzite, marble, minor phyllite, and carbonate as olistostromes. Alavi considered the sediments as deep water flysch deposits [7]. According to Abbasi [13], the first stage of regional metamorphism was low pressure and medium temperature (Staroulite zone within amphibolite facies).

Majidi [25] compared the meta-flysch with similar less metamorphosed, fossil-bearing rock exposed 150 Km southeast of Mashhad and given a Devonian-Carboniferous age. Eftekharnezhad & Behroosi [26] found Early Permian fossils form the same area studied by Majidi.

Slates are the most abundant meta-sedimentary rocks. Because of the complex structure, the thickness of the sedimentary can not be determined. The marble is about 10 to 40 m thick. Thin layers of marble are found in certain areas. Olistostroms are found as lenses in some areas such as Gholestan (near Vakilabad). The slaty cleavage is about N 40° W to N 45° W. Slate shows signs of two episodes of low-grade regional metamorphism.

The presence of different types of volcanic rocks as pebbles in the Per-Triassic conglomerate in Aghdarband area [23], and also Tuffaceous shale and pyroclastic rocks within the obducted remnants of the Paleo-Tethys in Binaloud, all indicate that the Paleo-Tethys oceanic crust was subducted northward under Turan plate and the volcanic arc formed along the margin of Turan plate.

Second low grade meta-sediments: To the southwest of major thrust fault (Fig. 1a) there is a thick sequence of low grade metamorphosed shale and

siltstone with a basal conglomerate. The conglomerate contains pebbles of ophiolite, meta-flysch, tonalite and granodiorite. The conglomerate is displaced by a thrust fault in the northern part (Fig. 1a). Due to thrusting, the basal conglomerate is highly sheared and silicified. Within the thrust zone there is a highly brecciated dolomite (Fig. 1a). The shale contains plant fossils which are dated Early Jurassic. The second regional metamorphism must have occurred after Early Jurassic.

Thrust faulting took place at different times from NE to SW. On the southern Binaloud, these slates are thrusted over Paleozoic and Tertiary rocks.

Jurassic conglomerate, sandstone and shale: Within a narrow NW-SE tectonic basin, conglomerates, shales, sandstone and siltstones were deposited (Fig. 1a). The basal conglomerate in the northern part of the basin changes into siltstone and shale in SW direction. The basal conglomerate contains pebbles and cobbles of meta-flysch, tonalite, granodiorite, and feldspar monzogranite porphyry. There are thin coal bearing horizons within the shale. Plant fossils are abundant. Higher up in the Jurassic section, there are conglomerate with rounded milky quartz pebbles. In SE direction near to leucogranite the quartz pebbles increase. Near Aghonj there is a quartz conglomerate with 90 percent rounded milky quartz. Most of the quartz pebbles originated from quartz veins formed during emplacements of granodiorite, feldspar monzogranite, and biotite-muscovite leucogranite.

Based on the following plant fossils, the age of this sequence is Lias-Dogger. Marattiopsis munsteri; Annulariopsis simpsoni; Cladophlebis whityensis; CL. Haiburnensis; Coniopteris hymenophylloides; Todites sp.; Nilssonia vittaeformis; Nilssonia polymoreha; N. petrophylloides; N. bozorga; N. harrisi; Petrophyllum tietzei; Anomozamites zirabiensis [27].

Early Cretaceous: Cretaceous rocks are exposed in the southern part of the study area (Fig. 1a). There are two rock types, a lower conglomerate and an upper limestone. The Cretaceous conglomerate contains interlayers of fossil bearing sandstones. Based on the fossils, an early Cretaceous age is proposed for this conglomerate. The conglomerate gradually changes into sandstone, sandy limestone, to massive limestone. Different types of fossils are found within the limestone. Based on some index orbitolina species, this limestone was deposited during Early Cretaceous time.

2.1. Regional and Contact Metamorphism

Two episodes of regional metamorphisms are recognized in the study area. The first stage took place during the initial stages of collision. It may be related to Hercynian orogeny which occurred in the Late Paleozoic. Only green schist facies rocks are exposed. Slates are dominated with minor phyllite. The second regional metamorphism occurred in Jurassic corresponding to Cimmerian orogeny. Exposed rocks are effected by the second regional metamorphism are of lower green schist facies.

Contact metamorphism is well developed around tonalite, granodiorite, feldspar monzogranite, and biotite-muscovite leucogranite (up to 300 m). Depending on the mineralogy and chemistry of the country rocks, different types of contact metamorphic rocks are formed. Mineralogical changes which are observed in an Al-rich slate outward from the contact of the intrusive rocks are: andalusite ± sillimanite ± k-feldspar ± cordierite, garnet, muscovite, biotite and spotted slate. Staurolite and choloritoid are formed in areas where the rocks were rich Fe, Mg and Al.

Based on k-feldspar and cordierite formed within the country rocks adjacent to granodiorite, a temperature of 660°C was calculated [13]. The contact metamorphism effect of biotite muscovite leucogranite was found to be about 500 to 550°C.

There is a bound of marble (20-30 m thick) within the meta-sediments. A small zone of skarn is developed at the hornblende- biotite- tonalite and marble contact (Fig. 1b).

Later tectonic activities such as folding and faulting changed the pattern of metamorphic isograds.

2.2. Tectonics

The Paleo-Tethys remnants are strongly affected by structural deformations at different times. The first deformation is either ductile or brittle-ductile thrust faults (T1) which transported the ophiolites from the north-northeast to south and emplaced them over the meta-flysch [8,9]. A mylonite zone is well developed between ophiolite and the meta-flysch. The first fold of S-verging with nearly horizontal axes (F1) affected the thrust.

The second thrust systems (T2) are brittle-ductile type and fault-bend folds are also associated with them [8,9]. They displaced both ophiolite and meta-flysch. Two types of folding affected the preexisting structures [8]. The F2 is tight isoclinal folds with nearly horizontal axes. Later thrusts are mainly brittle types. Thrusting is not being a continuous process. Structures which are formed before the Middle Jurassic are related to Cimmerian orogeny, whereas those formed after Late Cretaceous are related to Alpine structures [8]. The Quaternary thrusts and seismic activity indicate that the area is still active.

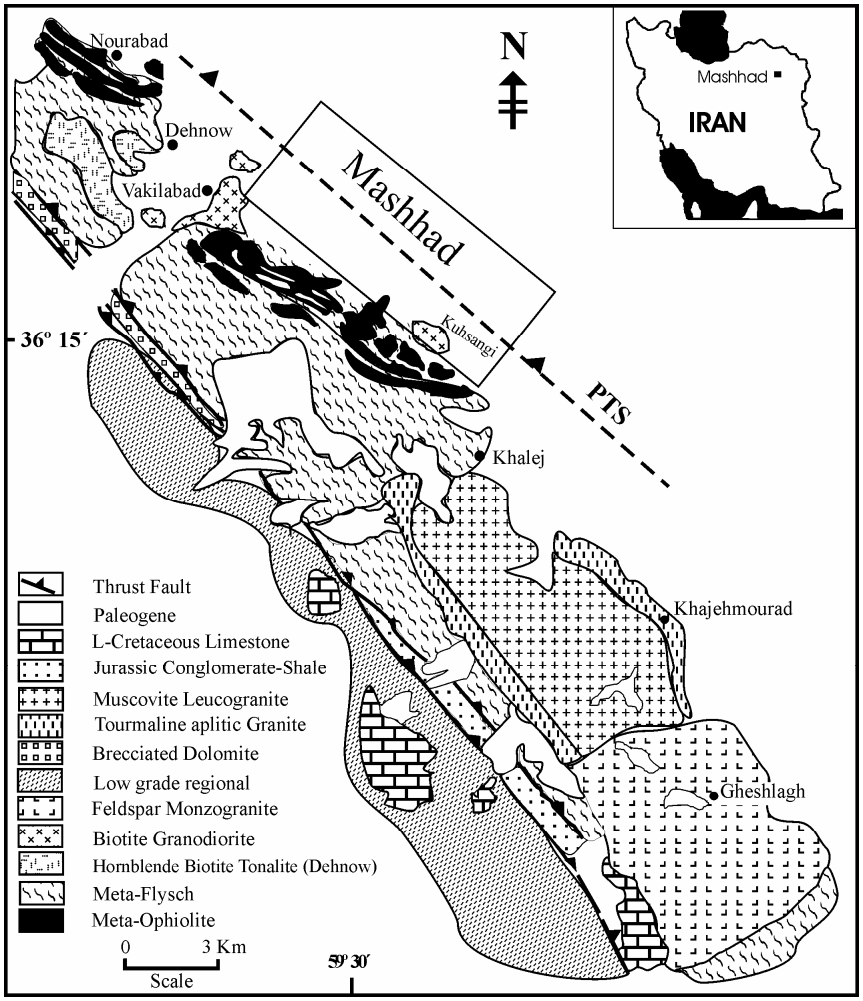

Figure 1a. Geological map of the study area. PTS refers to the Paleo-Tethys Suture zone.

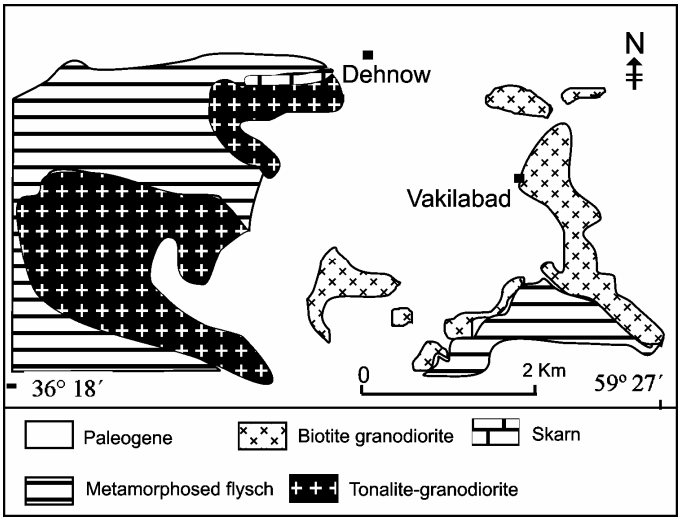

Figure 1b. Geological map showing the tonalite (Dehnow) and the granodiorite (Vakilabad).

3. Analytical Methods

Field work carried out in the plutonic metamorphic belt for over 10 years during teaching field geology course. During this period, more than 200 thin sections from the intrusives were studied. The area is very complicated due to several stages of regional and contact metamorphism. Intensive thrusting took place at different times, and different types of plutonic rocks intruded at different stages. After detailed petrographical studies, 21 samples of plutonic rocks were selected and analyzed for major, trace and rare earth elements. Major elements were analyzed by wavelength-dispersive X-ray fluorescence spectrometry (XRF) using fused discs. Pressed powder pellets were used for Zr, Nb, Sn, Sr, Ba, Sc, Y and Ga measurements by XRF at University of Colorado and Tasmania at Hobart, Australia.

REE composition of the rocks was determined by using ion exchange-X-ray fluorescence method developed by Robinson [29]. The XRF spectrometer used in this study was a Phillip PW 1410.

FeO and Fe_2O_3 content were determined by titration with standardized potassium permanganate solution with precision of ±1%. A Cameca SX 50 electron microprobe with WDS & EDS attachment at the Department of Earth Sciences, University of Colorado, and the Central Science Laboratory (CSL), University of Tasmania, was used for the analysis of biotite, muscovite and amphibole. The operation was at 15 kV and 20 nA with 10 s counting time.

Magnetic susceptibility of the rocks was measured by using GMS2 from geology department Ferdowsi University of Mashhad, Iran.

4. Petrography

4.1. Dehnow Hornblende Biotite Tonalite

The oldest igneous body intruded into the meta-ophiolite and meta-flysch is the Dehnow hornblendes-biotite- tonalite-granodiorite (Fig. 1b). Based on field observations, tonalite-granodiorite intruded after the first regional metamorphism and before Late-Triassic Early Jurassic. The Dehnow tonalite-granodiorite crops out in the northwestern part of the plutonic belt. It ranges from hornblende biotite tonalite to biotite granodiorite (Figs. 1a, b).

The hornblende biotite tonalite contains 35-50% plagioclase, 10 to 14% k-feldspar, 9-14% quartz, 15-11% biotite, less than 2% amphibole and in some places, minor clinopyroxene. Plagioclase displays weak zoning. Quartz is anhedral and occurs as interstitial grains. Biotite is the only peraluminous mineral present. Accessories minerals are apatite, zircon and ilmenite. Secondary minerals are chlorite, epidote and calcite.

Representative composition of biotite is reported in Table 1. The Fe-number [100Fe/(Fe + Mg)] is 62 and Al^{IV} is between 2.47-2.56. The titanium content of biotite, expressed as Ti atoms per formula unit, ranges from 0.32 to 0.351.

Plot of Al total *vs.* MgO (atoms per formula unit, [30] shows that biotites from Dehnow tonalite-granodiorite plot in the Calc-alkaline field (Fig. 2).

Amphiboles is ferrohornblende [Na + K] < 0.5 and Si = 6.62 (Fig. 3, Table 2) [31]. Experiments by Schmidt [32] have indicated that hornblende, when coexisting with biotite, plagioclase, titanite, magnetite and quartz, can be used a reliable geobarometer. Hornblende in biotite tonalite occurs in the same paragenesis. Based on Schmidt, [32] equation: P (±0.6 kb) = −3.01 + 4.76 $Al_{tot.}$

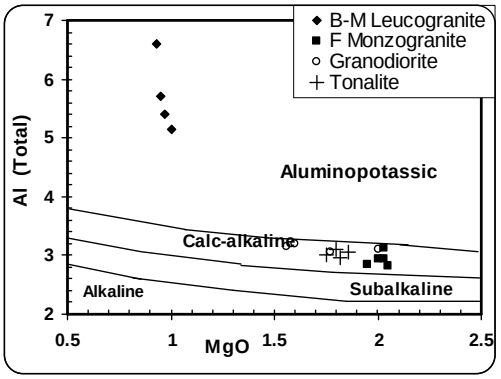

Figure 2. Al total *vs.* MgO (atoms per formula unit, after Nachit *et al.*, 1985) for biotites from different granitoids. Biotites from tonalite, granodiorite, and feldspar Monzogranite plot in the field of Calc-alkaline type and biotites from biotite-muscovite leucogranite plot in the field of aluminopotassic type.

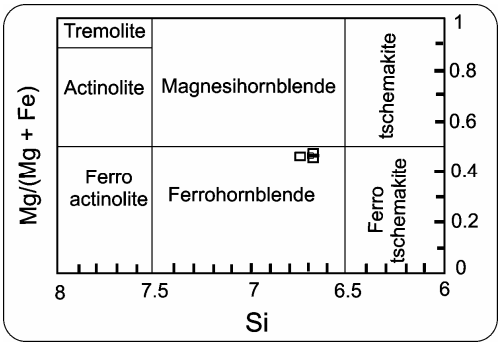

Figure 3. Classification of hornblende from tonalite in the diagram of Leake [31].

Table 1. Representative analyses of biotite from different intrusive

	Dehnow Tonalite		**Vakilabad Granodiorite**		**Kuhsangi Granodiorite**			**Feldspar Monzogranite**			**B-M Leucogranite**	
	V5-1	V5-2	T3-1	T3-2	X2-1	X2-2	X2-3	FG-1	FG-2	FG-3	MG-1	MG-2
SiO_2	35.75	34.75	35.76	35.98	35.4	34.17	34.96	35.77	36.04	35.67	30.9	26.21
TiO_2	3.02	2.72	0.51	2.51	2.26	2.18	2.42	2.583	2.47	2.197	2.92	2.3
Al_2O_3	16.3	16.60	17.61	16.84	17.47	16.85	16.60	15.874	15.33	17.263	29.34	37.94
Fe_2O_3	6.67	6.87	7.6	7.96	7.04	7.21	7.32	7.63	7.55	7.429	6.64	5.72
FeO	16.27	16.75	14.13	14.8	16.42	17.41	17.1	14.17	14.65	12.74	13.52	11.61
MnO	0.356	0.381	0.486	0.519	0.399	0.499	0.22	0.587	0.5	0.685	0.588	0.354
MgO	7.89	7.99	8.73	7.72	6.86	6.59	6.83	8.77	8.87	8.867	4.62	4.25
CaO	0.031	0.19	0.046	0.041	0.01	0.076	0.047	0.159	0.001	0.04	0.096	0.0718
Na_2O	0.14	0.135	0.07	0.088	0.046	0.061	0.12	0.069	0.07	0.115	0.112	0.189
K_2O	9.38	8.27	8.749	9.277	9.47	9.30	9.40	9.08	9.76	9.10	8.196	7.01
H_2O	3.79	3.69	3.80	3.70	3.83	3.69	3.75	3.70	3.66	3.78	3.61	3.844
F	0.112	0.246	0.011	0.316	0.004	0.09	0.078	0.304	0.40	0.248	0.867	0.424
Cl	0.121	0.094	0.092	0.12	0.086	0.09	0.07	0.018	0.008	0.013	0.001	0.045
Total	99.85	98.72	97.63	99.90	99.33	97.68	98.95	98.68	99.32	99.83	101.4	99.98
Si	5.528	5.439	5.59	5.553	5.507	5.452	5.5	5.565	5.60	5.48	4.599	3.875
Al^{IV}	2.472	2.561	2.41	2.447	2.493	2.458	2.5	2.435	2.4	2.52	3.41	4.125
Total Z	8	8	8	8	8	8	8	8	8	8	8	8
Al^{VI}	0.498	0.502	0.845	0.616	0.712	0.712	0.578	0.479	0.41	0.605	1.739	2.485
Ti	0.351	0.320	0.06	0.292	0.265	0.262	0.286	0.302	0.289	0.254	0.327	0.255
Fe^{3+}	0.866	0.897	0.994	1.027	0.916	0.96	0.963	0.994	0.982	0.952	0.828	0.642
Fe^{2+}	2.12	2.196	1.846	1.909	2.13	2.25	2.247	1.846	1.907	1.848	1.683	1.50
Mn	0.046	0.050	0.064	0.068	0.052	0.067	0.03	0.077	0.065	0.089	0.074	0.044
Mg	1.82	1.864	2.033	1.777	1.6	1.567	1.6	2.036	2.057	2.03	1.026	0.938
Total Y	5.701	5.829	5.842	5.689	5.675	5.818	5.704	5.734	5.71	5.778	5.677	5.864
Ca	0.005	0.042	0.007	0.007	0.002	0.013	0.008	0.0265	0.0002	0.006	0.015	0.011
Na	0.042	0.041	0.021	0.026	0.014	0.02	0.036	0.02	0.02	0.03	0.032	0.0544
K	1.85	1.653	1.744	1.826	1.88	1.89	1.88	1.804	1.936	1.784	1.556	1.323
Total X	1.897	1.736	1.772	1.859	1.896	1.923	1.924	1.8505	1.9562	1.82	1.603	1.3884
$Fe^*/Fe^* + Mg$	0.621	0.623	0.582	0.623	0.656	0.67	0.66	0.58	0.58	0.57	0.71	0.69

Biotite formulae were calculated based on 22 oxygen equivalents. Rocks are analyzed for Fe_2O_3 and FeO content using titration method and the Fe^{3+}/Fe^{2+} ratio in biotite is obtained based on this information

the calculated pressure of hornblende formation is 6 kbar (1 kbar = 100 MPa) corresponding to an estimated depth of about 22.5 km. Al-in-hornblende barometry suggests that early stage magmas resided at a pressure of 6 kbar before emplacement in the upper crust.

Xenoliths in the hornblende biotite tonalite are mainly derived from the country rocks, slates and meta-ophiolite.

Large garnet xenocrysts are found within the hornblende biotite tonalite near to the northern contact

where the country rocks are Fe-rich meta-pelites. The garnets are up to 2 cm in diameter and are of almandine type. The garnets are not homogeneous; they contain inclusions of biotite, quartz and plagioclase. These garnets originally were pieces of slates which were changed to garnet, biotite, quartz and plagioclase.

The hornblende biotite tonalite has a medium grained hypidimorphic texture. They commonly display a weakly to moderately foliation. This foliation does not follow the contact of the intrusive and has similar strike as the regional slaty cleavage. This fabric generally appears to be a result of regional metamorphism. The second regional metamorphism which occurred in Jurassic had affected hornblende biotite tonalite.

4.2. Biotite Granodiorite

Biotite granodiorite crops out in Vakilabad and Kuhsangi (Figs. 1a, b). Based on field observations, the granodiorite intruded after the first regional metamorphism, and before Late-Triassic-Early Jurassic. The biotite granodiorite contains 30-40% plagioclase, 13 to 18% k-feldspar, 15-27% quartz and 7-10% biotite. Plagioclase occasionally shows normal zoning. Quartz occurs as anhedral and interstitial grains. Biotite is also anhedral. Common accessory minerals include apatite, zircon and ilmenite. Secondary minerals are chlorite, calcite and minor epidote. Biotite granodiorite has a medium to fine-grained hypidimorphic texture. Biotite shows a foliation that follows the 2nd regional slaty cleavage.

Biotite is the only peraluminous mineral present in the granodiorite. Representative microprobe analyses of biotite from Vakilabad and Kuhsangi granodiorites are given in Table 1. The Fe-number [100Fe/(Fe + Mg)] is between 58 to 67 and Al^{IV} is between 2.41 to 2.5. The titanium content of biotite, expressed as Ti atoms per formula unit, ranges from 0·262 to 0.292.

Plot of Al total *vs.* MgO (atoms per formula unit, [31]) shows that biotites from Vakilabad and Kuhsangi granodiorite fall in the field of Calc-alkaline type (Fig.2).

4.3. Feldspar Monzogranite

Feldspar monzogranite is exposed in the southeastern plutonic belt (Fig. 1a). Based on field observations, feldspar monzogranite is younger than granodiorite and older than biotite-muscovite leucogranite. It contains 32 to 40%, quartz, 32 to 42%, k-feldspar, 8 to 17%, plagioclase, 5 to 10%, biotite and minor muscovite. Accessory minerals are scapolite, zircon and apatite. Feldspar granite has a coarse- grained texture with pink K-feldspar phenocrysts (2-3 cm long).

Table 2. Analysis of amphibole from Dehnow biotite tonalite and calculated pressure of formation

	D-1	**D-2**
SiO_2	43.21	43.9
TiO_2	1.07	0.95
Al_2O_3	10.50	10.42
Fe_2O_3	6.14	6.25
FeO	14.33	14.45
MnO	0.66	0.57
MgO	7.85	7.76
CaO	11.70	11.81
Na_2O	1.00	0.9
K_2O	1.03	1.1
H_2O	1.90	1.92
F	0.078	0.075
Cl	0.044	0.05
Total	99.512	100.155
Si	6.618	6.661
Al^{IV}	1.382	1.33
Total (T)	8	8
Al^{VI}	0.518	0.55
Ti	0.123	0.109
Fe^{3+}	0.786	0.794
Mg	1.791	1.773
Fe^{2+}	1.835	1.855
Mn	0.085	0.08
Ca	1.92	1.916
Na	0.299	0.267
K	0.202	0.214
$Mg/Fe^2 + Mg$	0.493	0.488
Total Al	1.896	1.88
P, kbar	5.98	5.93

Biotite is abundant. Representative microprobe analysis of biotite is given in Table 1. The Fe-number is between 57 to 58 and Al^{IV} is between 2.4 to 2.52. The titanium content of biotite, expressed as Ti atoms per formula unit, ranges from 0·254 to 0.302. Plot of Al total *vs.* MgO (atoms per formula unit, [30] shows that biotites from feldspar monzogranite plot of in the field Calc-alkaline type (Fig. 2). Muscovites are Al-rich (Table 3).

A weakly to moderately developed foliation fabric occurs in some areas which is formed by alignment of feldspars. This fabric seems to have formed by magmatic to possibly sub-magmatic processes with a weak solid-state overprint.

4.4. Tourmaline Aplite Granite

Biotite-muscovite leucogranite

Tourmaline aplitic granite intruded into the feldspar monzogranite and is found along the margin of biotite-muscovite leucogranite (Fig. 1a). Tourmaline is abundant in this intrusive rock. Garnet is also found with these rocks. Representative microprobe analyses of garnets are: 65.5-64.3% almandine, 15-16.7% grossularite, 12-12.34% pyrop, 5.6% spessartine and 2.4-2.8% andradite.

It is a batholith and forming NW/SE-elongated body with maximum dimensions of ~17 km and ~7 km. The batholith comprises different units: The border zone is mainly a tourmaline bearing aplite granite, biotite-muscovite leucogranite makes up the bulk of the batholith. Pegmatite dykes, which are locally abundant, are the youngest intrusive rocks and cut the biotite-muscovite leucogranite. It contains 35-38% quartz, 25-29% k-feldspar, 27-32% albite, 2.5-5% muscovite and 1.5-2.5% biotite. Common accessory minerals include tourmaline, garnet, apatite and zircon.

Aluminous biotite is the commonest ferromagnesian phase and accompanied by peraluminous phases: muscovite and garnet. Representative microprobe analyses of biotites are given in Table 1. The Fe-number is between 69 to 71 and AlIV is between 3.41 to 4.12. The titanium content of biotite, expressed as Ti atoms per formula unit, ranges from 0.25 to 0.327. Biotites in B-M leucogranite are Al-rich in comparison with tonalite and granodiorite. Plot of Al total *vs.* MgO (atoms per formula unit, [30]) shows those biotites from biotite-muscovite leucogranite plot in the field of aluminopotssic type (Fig. 2).

The biotite-muscovite leucogranite has a fine-grained equigranular texture and is poorly foliated. Xenoliths as angular blocks (some a large as 5 × 9 m) of the wall rocks are abundant in Khajehmourad area (Fig. 1a). The blocks show primary planner fabric and strong foliation. Different types of xenoliths are distinguished: feldspar monzogranite, metamorphic rocks, biotite granodiorite and micaceous rich fragments. Most of the xenoliths are feldspar monzogranite. At Khajehmourad, due to the abundance of very large feldspar monzogranite xenolith blocks within the biotite muscovite leucogranite, this could be the roof pendent area.

4.5. Pegmatites

Pegmatites are the youngest intrusive rocks in this belt. Numerous pegmatite dikes crosscut the older units. Most pegmatites dikes are small, they vary from 1 cm to as large as 25 m in width. Pegmatite dikes occur throughout the whole biotite-muscovite leucogranite plutonic complex and in the feldspar monzogranite (Fig. 1a). Small pegmatite dikes locally occur in granodiorite and tonalite. The grain sizes range from microscopic to several tens of centimeters. Microcline crystals measuring 40 cm long are formed.

The pegmatites can be classified based on their mineral content into 4-groups: Type-1 contains 60-90% pink microcline with minor albite as perthite (up to 20 cm long), 5-20% clear quartz, 5-20% muscovite (plates are 2-8 cm long) and in some areas up to 5% sericite as primary mineral forming radiating aggregates. Type-2 contains 70-80% pink microcline with some albite as perthite (up to 15 cm long), 10-15% quartz, 5% muscovite (up to 3 cm long) and 5% tourmaline (up to 12 cm long). Type-3 is less common and contains Microcline, quartz, muscovite, albite, almandine-type garnet and ± tourmaline. Type-4 is very rare and it contains microcline, quartz, muscovite, albite and beryl.

Pegmatites are being mined for feldspars. Feldspars are in general K-rich type, some Na-K feldspars are found in Khajehmourad area (Fig. 1a). Representative XRF analyses of feldspars from pegmatites are given in Table 4.

5. Geochemistry

5.1 Major and Trace Elements

Dehnow tonalite and granodiorite: Representative whole-rock major and trace element analyses for 20 rocks from different intrusive rocks are given in Table 5. Dehnow tonalite and granodiorite span a narrow range of SiO_2 content, from 55.1 to 58.16 wt %. Ternary plot of Ab-Or-An (after Barker, 1979) shows that Dehnow intermediate intrusive rocks plot in the field of tonalite-granodiorite (Fig. 4).

Plot of ($Na_2O + K_2O - CaO$) *vs.* wt % SiO_2 (after Frost [33] shows that Dehnow tonalite-granodiorites plot in the field of calcic-type with ($Na_2O + K_2O - CaO$) = −0.59 to −2.57 and they are sub-alkaline (Fig. 5). Plot of K_2O *vs.* wt % SiO_2 (after Rickwood, [34]) shows that Tonalite-granodiorite plot in the filed of High-K sub-alkaline type (Fig. 6a). The ratio of K_2O/Na_2O in tonalites are between 0.89-1.05 (Fig. 6b).

A discrimination plot of 1000 Ga/Al *vs.* Y and Zr + Ce + Y + Nb *vs.* ($Na_2O + K_2O$)/CaO (after Whalen *et al.*, [35] shows that tonalite-granodiorites plot within the field for I- and S-type granitoids (Figs. 7a, b).

Table 3. Representative analyses of muscovite

	F-monzogranite	**B-M-Granite**	
	FG-2	MG-1	MG-3
SiO_2	57.95	38.57	31.71
TiO_2	0	1.20	0.03
Al_2O_3	25.2	44.05	59.27
MgO	0	0.63	0.042
CaO	0.01	0.064	0.090
MnO	0	0.05	0
FeO	0.05	1.33	0.132
Na_2O	0.97	0.521	0.593
K_2O	13.75	8.82	7.164
H_2O	4.5	4.3	4.712
F	0.283	0.42	0
Cl	0.041	0.044	0.08
Total	102.77	100	103.823
Si	7.489	5.14	4.06
Al^{IV}	0.511	2.86	3.94
Total Z	8	8	8
Al^{VI}	3.32	4.05	4.9
Ti	0	0.125	0.003
Fe^{3+}	0.0001	0.043	0.004
Fe^{2+}	0.004	0.105	0.01
Mn	0	0.006	0
Mg	0	0.125	0.008
Total Y	3.3241	4.454	4.925
Ca	0.002	0.009	0.012
Na	0.244	0.134	0.146
K	2.26	1.5	1.157
Total X	2.506	1.643	1.315
$100(Fe^*+Mn)/(Fe^*+Mg+Mn)$	100	55.11	63.71

Table 4. Representative analyses of feldspars

	Gheshlagh	**Khajehmourad**	**Khajehmourad**
SiO_2	65.5-69.5	65.03	66.36-72.22
TiO_2	0.001	0.001	0.001
Al_2O_3	16.33-18.56	18.81	14.5-19.12
MgO	0.05	0.05	0.05
CaO	0.06-0.12	0.1	0.08-0.68
MnO	0.01	0.01	0.01-0.03
TFeO	0.06-0.1	0.22	0.16-1.4
Na_2O	2.4-2.65	2.97	1.96-7.78
K_2O	10.36-12.39	11.32	4.34-9.31
P_2O_5	0.03-0.13	0.14	0.04-0.15
L.O.I	0.54-0.72	0.9	0.87-1.05

Barbarin [36], classified granitoid rocks based on their origin and their geodynamic environments. Based on the classification, Dehnow tonalite-granodiorites belong to ACG (amphibole-rich calc-alkaline granitoids ACG) type (Fig. 8).

Villaseca, *et al.*, [37] divided peraluminous granites into 4-groups: 1) Highly peraluminous granitoids (h-P) which are typical S-type granites. They have the highest A = (Al-(K + Na +2Ca) (Fig. 9). They are characterized by having Al-rich minerals such as: muscovite, garnet (almandine- pyropeseries), cordierite and sillimanite. They usually contain abundant restitic enclaves, 2) Moderately peraluminous granitoids (m-P) (Fig. 9). Granitoids which plot in this filed are biotite bearing types. Accessory phases are cordierite and garnet (almandine-spessartine series). 3) Low peraluminous granitoids (L-P) (Fig. 9). They could be evolved from I-type or the low-ASI-type granitoids. They may contain amphibole. Enclaves are mainly mafic granular types. 4) Highly felsic peraluminous granitoids (F-P) (Fig. 9). Leucogranites belong to this series. They are usually two mica type and tourmaline bearing granitoids

Multi-cationic plot of Debon & Le Fort [38] and Villaseca *et al.*, [37] show that tonalite-granodiorites are meta-aluminous and fall in the field of I-type granites (Fig. 9). Dehnow tonalite-granodiorites have low values of magnetic susceptibility [(2-4) $\times$ 10^{-5} SI; which permits their classification in the ilmenite series of Ishihara, [39].

With increasing differentiation Index (D.I = percentage of normative quartz + albite + k-silicates); MgO, CaO, TiO_2 and FeO decrease linearly, and SiO_2, K_2O and Na_2O increase linearly (Table 5).

In general, granodiorites, feldspar granite and muscovite-biotite leucogranite are in the field of S-type granite.

Vakilabad and Kuhsangi granodiorite: Representative whole-rock major and trace element analyses for 8 rocks from different part of Vakilabad and Kuhsangi granodiorites are given in Table 5. Granodiorite spans a very narrow range of SiO_2 content, from 63.5 to 65.24 wt % (Table 5). Ternary plot of Ab-Or-An (after Barker, 1979) shows that Vakilabad and Kuhsangi intrusive rocks plot in the field of granodiorite (Fig. 4).

The Vakilabad-Kuhsangi granodiorites plot in the field of calcic-type with ($Na_2O + K_2O - CaO$) = 1.4-2 and they are sub-alkaline (Fig. 5). Plot of K_2O *vs.* wt % SiO_2 (after Rickwood, [34]) shows that Vakilabad-Kuhsangi granodiorite plot in the filed of High-K sub-alkaline type (Fig. 6a). The ratio of K_2O/Na_2O in granodiorite is between 0.84-1.26 and most of granodiorite plots in the filed of $K_2O > Na_2O$ (Fig. 6b).

Table 5. Major and trace elements analysis of representative rocks from different types of Mashhad Granites

Oxides %	**Dehnow V5**	**Dehnow V-1**	**Dehnow V-6**	**Dehnow V-2**	**Vakilabad T-1**	**Vakilabad T-2**	**Vakilabad T-3**	**Vakilabad S-1**	**Vakilabad S-2**	**Vakilabad P-2**
SiO_2	55.1	59.32	55.12	58.16	65.24	64.74	64.41	64.83	63.70	63.49
TiO_2	0.96	0.62	0.92	0.76	0.57	0.48	0.47	0.48	0.51	0.51
Al_2O_3	18.65	17.59	19.02	18.14	15.39	16.42	16.51	15.96	16.85	16.84
Fe_2O_3	1.95	1.59	1.44	1.86	1.85	1.16	1.40	1.18	1.20	1.71
FeO	6.70	4.77	7.15	5.58	4.41	3.95	3.86	3.96	3.96	3.78
MnO	0.16	0.14	0.2	0.16	0.11	0.13	0.13	0.12	0.13	0.13
MgO	3.01	2.60	2.7	2.32	1.89	1.79	1.68	1.85	1.71	1.88
CaO	6.99	5.69	7.25	6.13	3.84	4.28	4.25	3.78	4.18	4.01
Na_2O	2.46	2.48	1.9	2.71	2.41	3.0	2.74	2.84	3.03	2.72
K_2O	2.02	2.62	2.07	2.76	3.05	2.69	2.80	2.92	2.56	2.64
P_2O_5	0.32	0.20	0.23	0.22	0.19	0.18	0.16	0.14	0.18	0.20
H_2O (+)	1.7	1.34	1.9	1.4	1.26	1.2	1.2	1.68	1.14	1.35
H_2O (−)	0.16	0.16	0.15	0.15	0.12	0.12	0.13	0.19	0.22	0.16
Total	99.84	99.12	99.8	100.3	100.21	100.14	99.93	99.93	99.59	99.59
CIPW norms										
Q	10.29	16.66	17.55	12.41	26.61	23.27	24.48	24.5	23.10	24.95
C	0.40	0.78	1.33	0.02	1.57	1.19	1.62	1.59	1.92	2.70
Or	12.14	15.86	12.12	16.51	18.22	16.09	16.81	17.6	15.44	15.93
Ab	21.17	21.50	15.19	23.21	20.61	25.69	23.56	24.51	26.16	23.51
An	33.36	27.71	33.62	29.47	18.12	20.42	20.47	18.28	20.08	19.12
Hy	17.20	13.48	6.62	13.7	10.65	10.32	9.74	10.54	10.14	9.82
Mt	2.88	2.36	2.85	2.73	2.71	1.70	2.06	1.74	1.78	2.53
Il	1.85	1.21	1.71	1.46	1.09	0.92	0.91	0.93	0.99	0.99
Ap	0.77	0.49	0.65	0.53	0.45	0.43	0.39	0.34	0.44	0.48
D.I.	43.6	54.02	45.56	52.13	65.05	65.05	64.85	66.61	64.7	64.7
C.I.	3.19	4.39	3.8	4.0	5.89	6.29	6.25	6.56	6.27	6.27
Trace element (ppm)										
Sn	5	–	–	–	–	–	2	–	4.1	–
Rb	75	96	76	102	110.4	100	100	103.5	99	97
Sr	533	514	537	540	396	460	433	371	448	450
Ba	466	576	470	594	561	551	557	492	517	–
Nb	31.9	21.5	30.5	28.8	25.9	23.1	21.5	22.1	24.1	24
Zr	178	154	177	205	155	156	145	137	170	156
Ga	24	23	23.6	19	22	21	18	16	19	18
Y	24.2	18.7	22.4	–	15.4	15.2	21.2	14.3	15.4	20.5
Sc	–	13.97	–	–	–	–	9.19	9.06	–	–
Elemental Ratios										
Rb/Sr	0.14	0.18	0.14	0.18	0.27	0.21	0.23	0.27	0.22	0.2
Rb/Ba	0.16	0.16	0.16	0.17	0.19	0.18	0.18	0.209	0.19	–
K/Rb	111.77	114.45	112.6	112.29	115.06	110.85	116.2	117.08	106.55	113.06
Sr/Ba	1.14	0.892	0.92	0.865	0.263	0.835	0.777	0.754	0.866	–
Al_2O_3/TiO_2	19.4	28.37	20.65	23.8	27	34	35	33.3	33	33
CaO/Na_2O	2.84	2.3	3.81	2.26	1.59	1.42	1.55	1.33	1.38	1.47
Ca/Sr	93.50	78.92	96.3	80.93	69.69	66.34	69.88	72.64	66.52	63.53
K/Na+K	0.55	0.54	0.52	0.53	0.58	0.50	0.53	0.53	0.48	0.52
C/ACF	0.28	0.29	0.29	0.29	0.26	0.28	0.27	0.25	0.27	0.26
A/CNK	1.037	1.01	1.01	0.974	1.077	1.049	1.049	1.089	1.09	1.1
Mt. Susceptibility (SI)	2.5×10^{-5}	2.1×10^{-5}	2.6×10^{-6}	2×10^{-5}	1.9×10^{-5}	1.8×10^{-5}	1.8×10^{-5}	1.9×10^{-5}	2×10^{-5}	2.5×10^{-5}

Table 5. Continued

Oxides %	Kuhsangi X-1	FG-1	FG-4	FG-5	MG-1	MG-3	MG-4	MG-B	AG-1	AG-2
SiO_2	63.97	67.48	68.59	67.2	73.27	72.64	72.08	72.39	73.62	74.27
TiO_2	0.51	0.45	0.39	0.41	0.18	0.18	0.21	0.22	0.06	0.05
Al_2O_3	17.16	15.76	15.65	15.5	14.45	14.52	14.81	14.61	14.88	14.77
Fe_2O_3	1.40	0.81	0.73	0.75	0.34	0.42	0.4	0.34	0.20	0.15
FeO	3.69	2.25	2.07	2.15	1.08	1.03	1.21	0.99	0.65	0.55
MnO	0.12	0.10	0.08	0.09	0.03	0.04	0.03	0.04	0.04	0.14
MgO	1.32	1.08	1.0	1.1	0.35	0.33	0.25	0.29	0.23	0.16
CaO	4.77	2.13	2.19	2.14	1.0	1.03	1.04	0.98	0.56	0.83
Na_2O	2.75	3.49	3.57	3.45	3.70	3.57	3.2	3.23	4.61	4.33
K_2O	2.81	4.58	4.17	4.52	5.09	4.77	5.19	5.03	3.72	4.24
P_2O_5	0.20	0.10	0.25	0.15	0.15	0.19	0.18	0.16	0.17	0.10
H_2O (+)	1.18	1.04	0.91	1.1	0.78	0.84	1.34	1.09	1.34	0.62
H_2O (−)	0.11	0.14	0.13	0.12	0.12	0.12	0.18	0.09	0.18	0.22
Total	99.99	99.41	99.73	99.78	100.51	99.68	99.49	99.46	99.46	100.31
CIPW norms										
Q	23.56	25.31	25.42	22.79	29.42	31.2	31.16	32.21	31.39	30.73
C	1.85	1.43	1.84	1.4	1.36	2.05	2.46	2.46	2.65	1.77
Or	16.83	27.26	24.97	26.68	30.19	28.56	31.11	30.25	22.26	25.16
Ab	23.58	29.74	30.61	29.16	31.42	30.60	27.46	27.81	39.51	36.79
An	22.78	9.91	9.52	9.68	4.09	4.04	4.16	3.99	1.80	3.54
Hy	8.40	5.67	5.26	5.55	2.34	2.17	2.25	2.0	1.60	1.47
Mt	2.06	1.18	1.07	1.09	0.49	0.62	0.59	0.50	0.29	0.22
Il	0.98	0.82	0.75	0.78	0.34	0.35	0.40	0.43	0.12	0.10
Ap	0.48	0.24	0.6	0.33	0.36	0.46	0.43	0.39	0.41	0.24
D.I.	63.93	82.31	81.0	78.63	91.03	90.36	89.73	90.27	90.27	93.16
C.I.	6.21	12.01	12.74	12.24	29.62	28.81	27.74	31.01	31.01	49.96
Trace element (ppm)										
Sn	–	5.1	6	–	7	–	7	–	–	14
Rb	105	180.8	181.5	181.2	235.4	261.3	253.9	239.6	239.6	265.1
Sr	418	584.2	535	543	204.8	205.5	236.4	236	236	53
Ba	550	1093	886	968	611	556	708	771	771	138
Nb	23.7	40.9	50.1	46.2	25.2	27.9	26.5	28.7	28.7	20.4
Zr	187	188	182	187	115	109	132	130	130	30
Ga	16	20	18	17.8	18	20	22	19	8	5
Y	14.1	15.4	15.7	15.6	8.3	10.4	8.5	6.7	6.7	10.6
Sc	7.41	5.12	4.78	–	1.85	1.83	–	2.21	2.21	–
Elemental Ratios										
Rb/Sr	0.25	0.3	0.33	0.32	1.15	1.27	1.07	1.01	1.01	5
Rb/Ba	0.19	0.16	0.204	0.18	0.38	0.46	0.35	0.31	0.31	1.92
K/Rb	111.06	105.12	95.34	97.7	65.34	75.75	84.83	87.12	87.12	58.23
Sr/Ba	0.76	0.534	0.603	0.56	0.385	0.369	0.333	0.30	0.306	0.384
Al_2O_3/TiO_2	33.6	35	40	28.9	80.3	80.6	70.4	66.40	248	295.4
CaO/Na_2O	1.73	0.61	0.61	0.62	0.27	0.28	0.32	0.30	0.12	0.19
Ca/Sr	81.28	25.99	29.18	26.7	34.83	35.73	31.67	29.60	29.60	75.33
K/Na+K	0.52	0.57	0.56	0.56	0.606	0.606	0.64	0.635	0.635	0.47
C/ACF	0.30	0.24	0.26	0.24	0.24	0.22	0.21	0.22	0.22	0.16
A/CNK	1.056	1.08	1.086	1.07	1.077	1.134	1.159	1.164	1.164	1.177
Mt. Susceptibility (SI)	1.5×10^{-5}	–	2.3×10^{-5}	2.4×10^{-5}	0×10^{-5}	2×10^{-5}	1×10^{-5}	–	–	1×10^{-5}

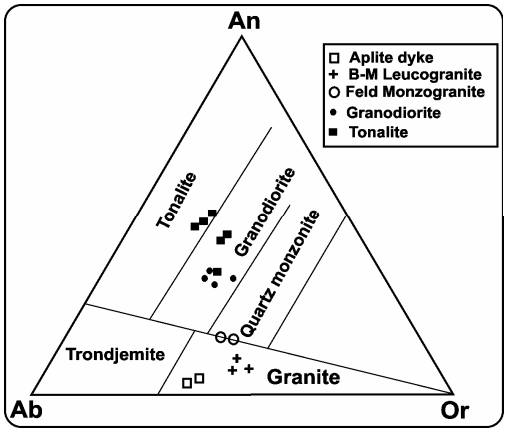

Figure 4. CIPW normative Ab-An-Or granitic rock classification after Barker [40].

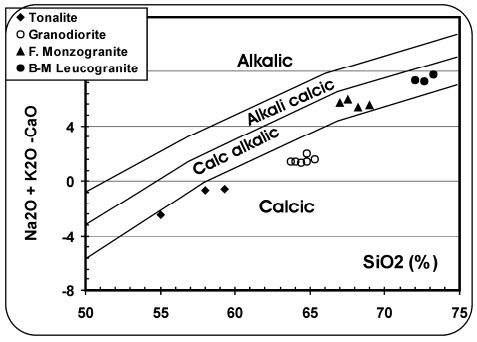

Figure 5. Plot of SiO_2% *vs.* ($Na_2O + K_2O - CaO$) [33] shows that Dehnow tonalite granodiorite and Vakilabad-Kuhsangi granodiorites plot in the field of Calcic-type and feldspar Monzogranite and biotite-muscovite leucogranite plot in the field of calc-alkalic-type.

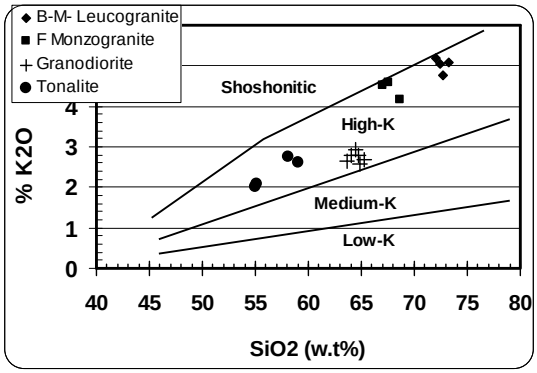

Figure 6a. Plot of SiO_2% *vs.* K_2O [34] shows that all of the Mashhad granitoid rocks plot if the filed of High-K sub-alkaline type.

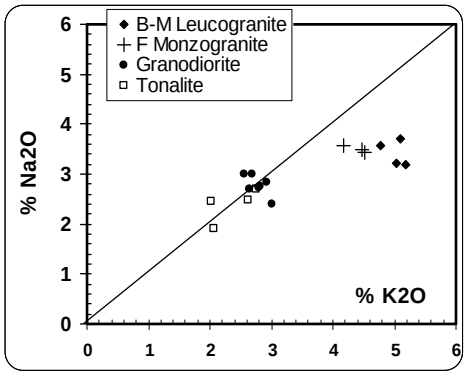

Figure 6b. Plot of Na_2O % *vs.* K_2O shows that feldspar Monzogranite and biotite-muscovite leucogranite have the highest K_2O/Na_2O ratio (1.31-1.62); tonalite and granodiorite have K_2O/Na_2O ratio around 1±0.1.

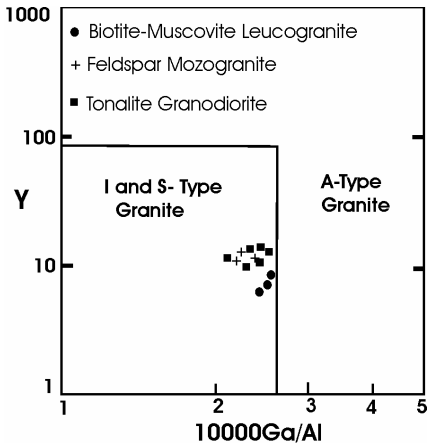

Figure 7a. Y *vs.* 10000Ga/Al discrimination plot for tonalite-granodiorite, Feldspar granite, and muscovite biotite granite [33]). All of Mashhad granitoid rocks plot in the field of I-S type granites.

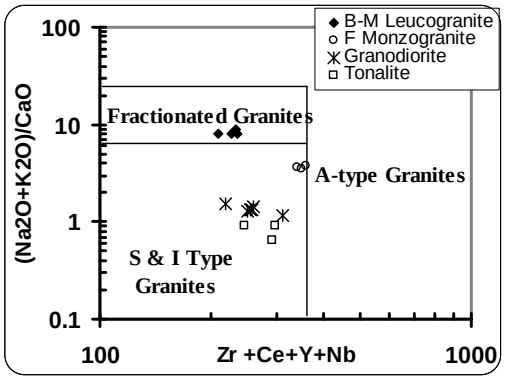

Figure 7b. Zr + Ce + Y + Nb *vs.* (Na2O + K2O)/CaO discrimination plot for tonalite-granodiorite, Feldspar granite, and muscovite biotite granite [33]. Tonalite, granodiorite, and feldspar Monzogranite plot in the field of I-S type granites, Biotite-muscovite leucogranite plots in the field of fractionated granites.

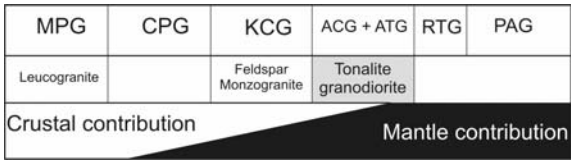

Figure 8. Diagram showing Barbarin [36] Classification of granitoids rocks based on their origin and their geodynamic environments. Dehnow tonalite and Vakilabad-Kuhsangi granodiorite belong to ACG (amphibole-rich calc-alkaline granitoids ACG) type; Feldspar monzogranite belongs to KCG (K-rich calc-alkaline granitoids KCG) type; and biotite-muscovite leucogranite belongs to MPG (muscovite-bearing peraluminous granitoid) type.

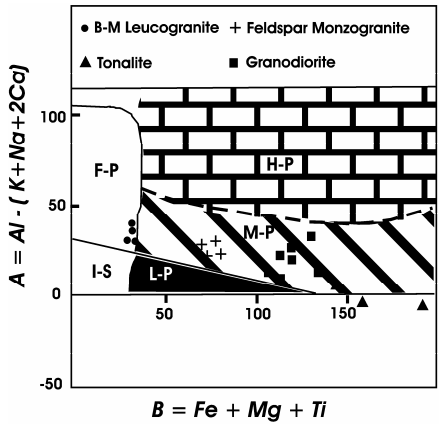

Figure 9. Multi-cationic plot of Debon & Le Fort [38] and field of peraluminous granites (L-P = low peraluminous, M-P = medium peraluminous, H-P = high peraluminous, and FP = felsic peraluminous; I-S is the boundary line between I- and S-type granites) [37] showing that Dehnow tonalite-granodiorite are meta-aluminous, Vakilabad-Kuhsangi granodiorites and feldspar monzogranites plot in the field of medium peraluminous, and muscovite-biotite leucogranite plots it the filed of felsic peraluminous.

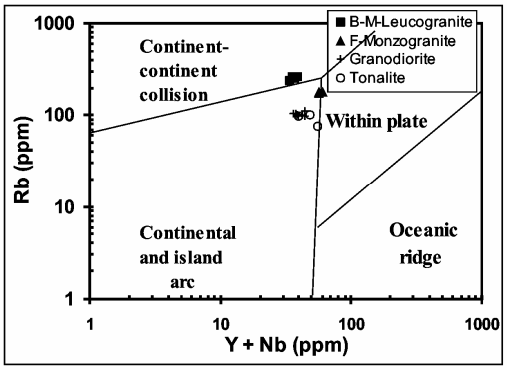

Figure 10. Rb *vs.* Y+Nb discrimination plot [41] show that Dehnow tonalite and Vakilabad-Kuhsangi granodiorites plot in the filed of arc related intrusive rocks; Feldspar Monzogranite plot in the boundary filed of arc and within plate magmatism and biotite-muscovite leucogranite plot in the field of collision setting.

The Vakilabad-Kuhsangi granodiorites plot within the field for I- and S-type granitoids.

Based on Barbarin [36] classification, Vakilabad-Kuhsangi granodiorites belong to ACG (amphibole-rich calc-alkaline granitoids ACG) type (Fig. 8).

The Vakilabad and Kuhsangi granodiorites plot in the field of moderately peraluminous granitoids (M-P) (Fig. 9) Since they are above the I-S line (Fig. 9) therefore they are S-type granitoid. Vakilabad and Kuhsangi granodiorites have low values of magnetic susceptibility [(1.5 to 4.5) × 10^{-5} SI; which permits their classification in the ilmenite series of Ishihara, [39]

Differentiation Index (D.I) changes very slightly; D.I = 63.93-66.54 (Table 5).

Feldspar Monzogranite: Elemental analyses from feldspar monzogranite are presented in Table 5. Ternary plot of Ab-Or-An [40] shows that feldspar monzogranite plotting within the boundary of granite and quartz monzonite; therefore they are named as feldspar monzogranite (Fig. 4).

The feldspar monzogranite plot in the field of calc-alkaline type with ($Na_2O + K_2O - CaO$) = 5.4-5.95 and they are sub-alkaline (Fig. 5). Plot of K_2O *vs.* wt % SiO_2 (after Rickwood, [34]) shows that feldspar monzogranite plot in the filed of High-K calc-alkaline type (Fig. 6a). The ratio of K_2O/Na_2O in feldspar monzogranite is between 1.16-1.31 (Fig. 6b).

Differentiation Index (D.I) changes very slightly; D.I = 81 to 82.3 (Table 5).

The feldspar Monzogranite plot within the field for I- and S-type granitoids (Figs. 7a, b).

Based on Barbarin classification, feldspar monzogranite belongs to KCG (K-rich calc-alkaline granitoids KCG) type (Fig. 8).

The Feldspar Monzogranite plot in the field of moderately peraluminous granitoids (M-P) (Fig. 9).

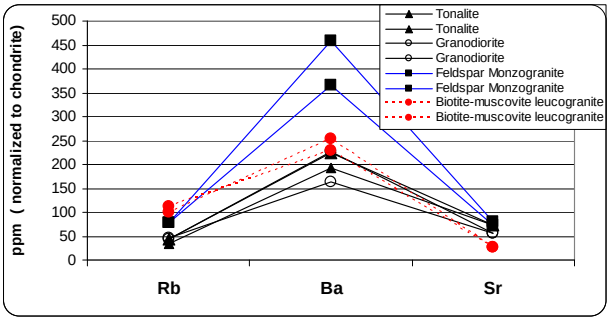

Figure 11. Rb, Ba, and Sr diagram normalized to chondrite (Sun and McDonough 1989). Feldspar granite has highest Ba and tonalite-granodiorites have the lowest Ba content. Muscovite-biotite leucogranite has the highest Rb and lowest Sr.

Since they are above the I-S line (Fig. 9) therefore they are S-type granitoid. Feldspar monzogranite have low values of magnetic susceptibility [(2-3) × 10^{-5} SI; which permits their classification in the ilmenite series of Ishihara [39].

Biotite-Muscovite leucogranite: Elemental analyses from Biotite-Muscovite leucogranites are presented in Table 5. SiO_2 content changes from 72 to 74.27 wt % (Table 5). Ternary plot of (Ab-Or-An) [40] shows that Biotite-Muscovite leucogranites plotting in the field of granite (Fig. 4).

The biotite-muscovite leucogranite plot in the field of calc-alkaline type with ($Na_2O + K_2O - CaO$) = 7.3-7.8 and they are sub-alkaline (Fig. 5). Plot of K_2O *vs.* wt % SiO_2 (after Rickwood, [34]) shows that biotite-muscovite leucogranite plot in the filed of High-K calc-alkaline type (Fig. 6a). The ratio of K_2O/Na_2O in biotite-muscovite leucogranite is between 1.33-1.62 (Fig. 6b). Differentiation Index (D.I) changes very slightly; D.I = 89 to 91 (Table 5).

The biotite-muscovite leucogranite plot within the field for I- and S-type granitoids is shown in Fig. 7a. A discrimination plot of (Zr + Ce + Y + Nb) *vs.* ($Na_2O + K_2O$)/CaO (after Whalen *et al.*, [35]) shows that biotite-muscovite leucogranite plotting in the field of fractionated granite (Fig. 7b)

Based on Barbarin classification, biotite-muscovite leucogranite belongs to a MPG (muscovite-bearing peraluminous granitoid) type (Fig. 8).

The Biotite-muscovite leucogranite plot if the filed of highly felsic peraluminous granitoids (F-P*)* (Fig. 9). They are S-type granitoid. Biotite-muscovite leuco-granites have low values of magnetic susceptibility [(0 to 1) × 10^{-5} SI; which permits their classification in the ilmenite series of Ishihara [39].

The Rb *vs.* Nb+Y discrimination diagram of Pearce *et al.*, [39] shows that Dehnow tonalite-granodiorite, Vakilabad-Kuhsangi granodiorite and feldspar monzogranite samples plot in the Continental and arc-granite field, (Fig. 10). Biotite-muscovite leucogranite plot in the field of syn-collision granite is shown in Syn-COLG, Figure 9.

The low field strength elements (LFSE) (Rb, Ba and Sr) content of Mashhad granitoids are in general high (Table 5). Tonalite has the lowest Rb ≈75 to 102 ppm and biotite-muscovite leucogranite has the highest Rb ≈235-261 ppm (Fig. 11). The Rb/Sr is between 0.14 to 0.18 in tonalite, 0.20 to 0.27 in granodiorite, 0.3 to 0.33 in feldspar monzogranite and 1.07 to 1.27 in biotite muscovite leucogranite (Table 5). The Ba content of tonalite and granodiorite is between 460 to 590 ppm, in biotite-muscovite leucogranite is between 550 to 708 ppm and feldspar monzogranite has the highest Ba = 886-093 ppm (Table 5). The Ba content of both feldspar Monzogranite and biotite-muscovite leucogranite is very high (Fig. 11). This indicates that the K-feldspar content of the source rock was high and they were totally melted.

REE analyses of selected samples from different intrusives are shown in Table 6. In general, tonalite and granodiorite exhibit similar chondrite-normalized REE patterns (Fig. 12a), which are characterized by moderate light rare earth element (LREE) enrichment, low heavy REE (HREE) and small negative or no Eu anomalies (Eu/Eu* = 0.74 to 1.1).

Table 6. Rare earth elemental analyses and characteristic rare earth ratios of the Mashhad granits

REE (ppm)	Dehnow V-1	Vakilabad T-3	Vakilabad S-1	KuhsangI X-1	FG-1	FG-4	MG-1	MG-3	MG-B	AG-2
La	28.06	30.17	20.81	37.94	61.2	54.93	41.48	32.3	42.42.	8.25
Ce	58.95	62.58	44.62	85.97	115.1	101.15	84.68	61.37	83.33	16.45
Pr	6.22	6.57	4.69	8.51	11.15	9.72	8.73	6.23	9.23	1.83
Nd	22.31	21.88	17.37	30.55	35.86	31.46	28.21	19.19	29.63	6.35
Sm	4.83	3.88	3.81	6.05	5.27	5.09	4.81	4.18	5.61	1.86
Eu	1.37	0.89	1.23	1.55	0.85	1.08	0.65	0.88	1.01	0.55
Gd	3.85	3.33	2.91	4.24	3.27	3.29	2.53	2.66	3.07	2.16
Dy	3.66	3.52	2.79	2.93	2.76	2.73	1.8	2.18	1.88	4.46
Er	2.27	2.05	1.57	1.47	1.34	1.51	0.64	0.96	0.85	3.89
Yb	1.77	2.03	1.35	1.23	0.97	1.13	0.24	0.66	0.49	4.99
Sum	133.29	136.9	101.15	180.44	237.77	212.09	173.77	130.61	177.52	50.79
REE ratios										
(La/Yb)N	11.38	10.6	6.38	22.13	45.3	38.89	125	37.24	62.14	1.18
La/Eu	7.7	7.78	3.88	5.58	16.46	11.6	14.6	8.5	9.6	3.44
Eu/Eu*	0.95	0.74	1.1	0.9	0.59	0.77	0.52	0.76	0.68	0.84

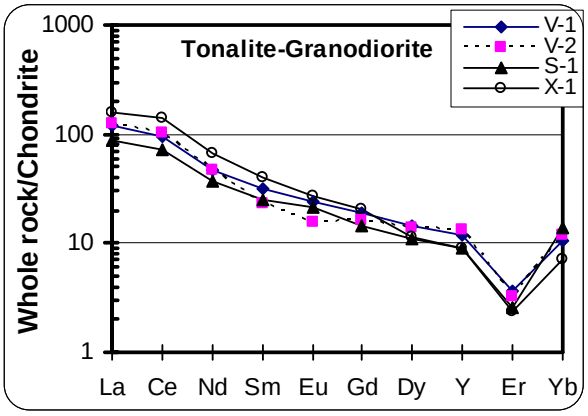

Figure 12a. Chondrite-normalized REE distribution for tonalite and granodiorite.

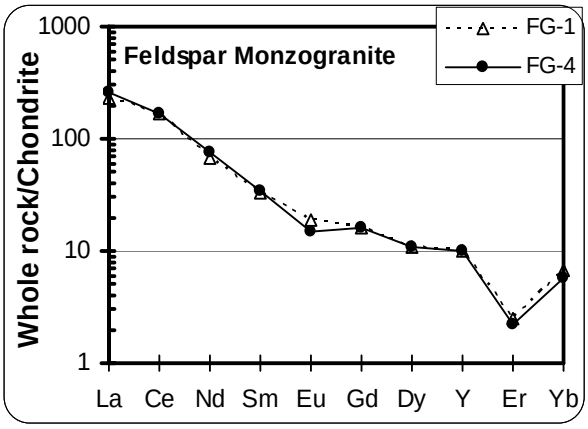

Figure 12b. Chondrite-normalized REE distribution for feldspar monzogranite.

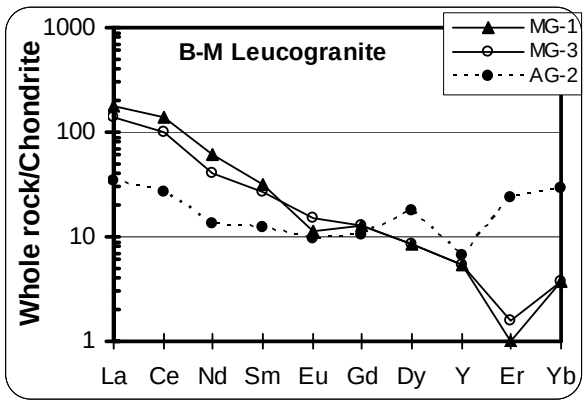

Figure 12c. Chondrite-normalized REE distribution for biotite-muscovite leucogranite and aplitic dikes.

Chondrite-normalized REE patterns (Fig. 12b), of feldspar monzogranite characterized by strong light rare earth element (LREE) enrichment and less low heavy REE (HREE) in comparison with tonalite and granodiorite. All samples have small negative Eu anomalies (Eu/Eu* = 0.59 to 0.77).

Chondrite-normalized REE patterns (Fig. 12c), of biotite-muscovite leucogranite characterized by moderate light rare earth element (LREE) enrichment and very low heavy REE (HREE) in comparison with tonalite-granodiorite and feldspar monzogranite. All samples have negative Eu anomalies (Eu/Eu* = 0.52 to 0.76).

The (La/Yb)N *vs.* Eu/Eu* diagram shows that biotite-muscovite leucogranite has the highest [(La/Yb)N = 37-124] and tonalite-granodiorite has the lowest [(La/Yb)N = 7 to 22] (Fig. 13). Tonalite and granodiorite has very small negative to no Eu anomalies (Eu/Eu* = 0.74 to 1.1). Feldspar monzogranite and biotite-muscovite leucogranite have similar small negative Eu anomalies (Eu/Eu* = 0.52 to 0.77) (Fig. 13). Total REE content of tonalite and granodiorite is between 101 to 136 ppm, in feldspar monzogranite having the highest, is 221-238 ppm and in biotite-muscovite leucogranite is 130-170 ppm (Table 6).

Rock/chondrite normalized spidergrams of representative samples of different Mashhad granitoids are plotted in Figures 14a-d. Well defined negative anomalies are observed for P, Ti and Er. Biotite-muscovite leucogranite has the highest negative anomalies for Ti and Er and tonalite-granodiorite have the lowest anomalies (Fig. 14a). Fractionation or presence of some minerals in the restites will explain the negative anomalies: apatite (P), ilmenite and/or titanite (Ti) and garnet (Er).

LFSE elements (Sr and Ba) show positive anomalies (Fig. 14a). Ba shows the highest positive anomaly (Fig. 14a). High field strength elements (HFSE) Zr, Nb and Ce, show small positive anomalies (Fig. 14a).

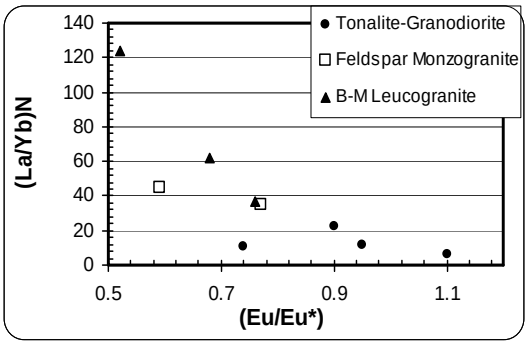

Figure 13. Plot of (La/Yb)n *vs.* (Eu/Eu*) showing that biotite-muscovite leucogranite has the highest (La/Yb)n ratio.

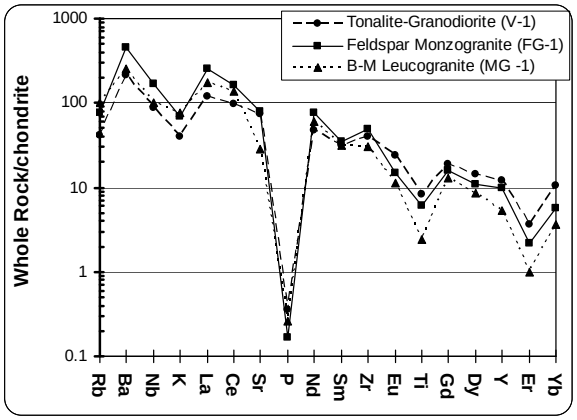

Figure 14a. Rock/chondrite normalized spidergrams of selected sample from tonalite, granodiorite, feldspar Monzogranite, and biotite-muscovite leucogranite.

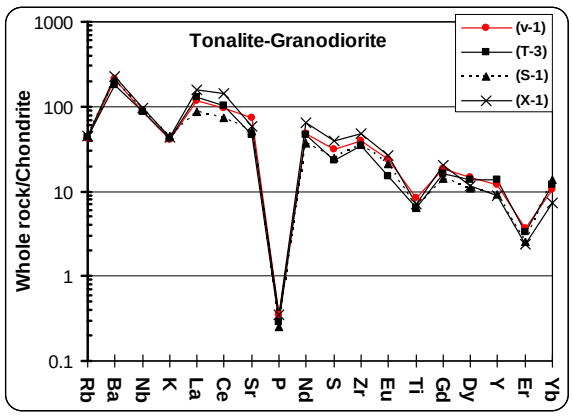

Figure 14b. Rock/chondrite normalized spidergrams of representative sample from tonalite and granodiorite.

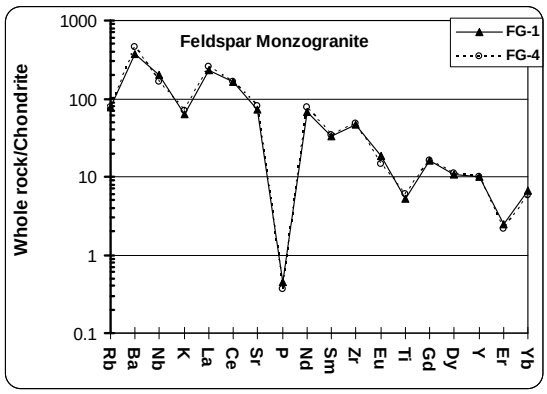

Figure 14c. Rock/chondrite normalized spidergrams of representative sample from feldspar monzogranite.

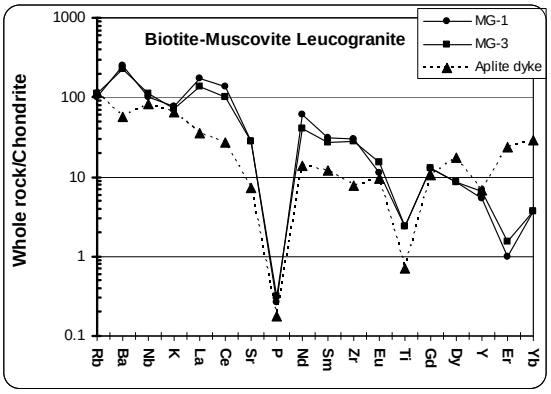

Figure 14d. Rock/chondrite normalized spidergrams of representative sample from biotite-muscovite leucogranite and aplitic dikes.

6. Conclusions

• The Paleo-Tethys opened in Silurian time (The Binaloud range in northeastern Iran, south of Mashhad, is a remnant of Paleo-Tethys).

• Subduction of Paleo-Tethys oceanic crust under Turan plate started in Late Devonian and continued into Triassic and led to the formation of a volcanic arc [23].

• Major porphyry Cu-Au were formed along this arc in Uzbekistan and Kazakhstan.

• By the opening of the Neo-Tethys, Iranian Plate collided with the Turan Plate.

• By the late Carnian (about 225 m.y. ago) there was no Paleotethys left on an Iranian transect.

• The abducted remnants of the Paleo-Tethys Ocean in Binaloud range, Iran, include several rock assemblages including ophiolite complexes, Meta-flysch and some submarine pyroclastics.

• Hercynian orogeny (Late Paleozoic) and Cimmerian orogeny (Jurassic) cased two episodes of regional metamorphisms.

• REE and trace element data support the field relationships that the Paleo-Tethys remnants (meta-ophiolite and meta-flysch) were intruded at three different episodes of magmatism (Triassic to Cretaceous time). 1) Dehnow-Kuhsangi hornblende biotite tonalite-granodiorite, 2) Sangbast Feldspar monzogranite, and 3) Khajehmourad biotite-muscovite leucogranite and pegmatite.

Dehnow to Kuhsangi tonalite-granodiorite (Early Triassic) are meta to moderately peraluminous S to I-type granitoids. They are sub-alkaline, calcic-type. They have low values of magnetic susceptibility [(1.5 to 2.5)×10^{-5} SI]. Feldspar Monzogranite (Late Triassic) is moderately peraluminous, K-rich calc-alkaline type. Biotite-muscovite leucogranite and late pegmatite dikes (Jurassic age) are highly felsic peraluminous S-type granitoids. They are syn-collision granite. They have low values of magnetic susceptibility [(0.1 to 0.6)×10^{-5} SI].

Tonalite and granodiorite exhibit similar chondrite-normalized REE patterns which are characterized by moderate light rare earth element (LREE) enrichment, low heavy REE (HREE) and small negative or no Eu anomalies (Eu/Eu* = 0.74 to 1.1). Feldspar monzo-granite characterized by strong light rare earth element (LREE) enrichment and less low heavy REE (HREE) in comparison with tonalite and granodiorite. All samples have small negative Eu anomalies (Eu/Eu* = 0.59 to 0.77). Biotite-muscovite leucogranite characterized by moderate light rare earth element (LREE) enrichment and very low heavy REE (HREE) in comparison with tonalite-granodiorite and feldspar monzogranite. All samples have negative Eu anomalies (Eu/Eu* = 0.52 to 0.76).

Total REE content of tonalite-granodiorite is 101-136, in feldspar monzogranite is 221-238 and in leucogranite is 130-170 ppm. The leucogranite has the highest [(La/Yb)N = 37-124] tonalite-granodiorite has the lowest [(La/Yb)N = 7 to 22]. The Eu anomalies (Eu/Eu* = 0.55 to 1.1) is low in all of them.

Rock/chondrite normalized spidergrams of representative samples of different Mashhad granitoids has well defined negative anomalies for P, Ti and Er. Biotite-muscovite leucogranite has the highest negative anomalies for Ti and Er and tonalite-granodiorite have the lowest anomalies. Fractionation or presence of some minerals in the restites will explain the negative anomalies: apatite (P), ilmenite and /or titanite (Ti) and garnet (Er).

LFSE elements (Sr and Ba) show positive anomalies. Ba shows the highest positive anomaly. High field strength elements (HFSE) Zr, Nb and Ce, show small positive anomaly.

Tonalite-granodiorite magma originated from a mafic source. Feldspar monzogranite originated from a deeper source and contaminated in the crust. Leucogranite may have originated from the crustal materials.

Acknowledgments

The authors wish to thank Dr Ross R Large director of Centre for Ore Deposit Research, University of Tasmania, Hobart, Australia for accessing to use the research facilities. Thanks to people working in Central Sciences Laboratory, University of Tasmania for electron microprobe analysis.

We are grateful to reviewers and referees of Journal of Sciences Islamic Republic of Iran, which helped to refine the article.

References

1. Jarchovski T., Momenzadeh M., Tadayon A., and Ziegler V. Mineral reconnaissance in Mashhad Quadrangle. *Geol. Surv. of Iran*, p. 192 (1973).
2. Alberti A. and Moazez. Z. Plutonic and metamorphic rocks of the Mashhad area (northeastern Iran, Khorasan). *Boll. Soc. Geol. Italy*, **93**: 1157-1196 (1974).
3. Alberti A., Nicoletti M., and Petrucciani C. K-Ar Ages of micas of Mashhad granites. *Period Miner.*, **42**: 483-493 (1973).
4. Plimer I.R. and Moazez Lesco Z. Garnet xenocrysts in the Mashhad Granite, NE Iran. *Geologische Rundschau.*, **69**(3): 801-810 (1980).
5. Majidi B. The geochemistry of ultrabasic and basic lava flows occurrences in northeastern Iran, In Geodynamic project in Iran. *Geological Survey of Iran*, Report No. 51, 463-477 pp. (1983).
6. Alavi M. The Virani ophiolite complex and surrounding rocks. *Geology Rundsch.*, **68**: 334-341 (1979).
7. Alavi M. Sedimentary and structural characteristics of the Paleo-Tethys remnants in northeastern Iran. *Geological Society of America Bulletin*, **103**(8): 983-992 (1991).
8. Alavi M. Thrust tectonics of the Binaloud region; NE Iran. *Tectonics*, **11**(2): 360-370 (1992).
9. Karimpour M.H. Application of Sm/Eu, Rb, Ce/Yb, and E-Rb to discriminate between tin-mineralized and non-mineralized S-type granites. *Scientific Quarterly Journal Geosciences*, **7**(29): 1-16 (1999).
10. Karimpour M.H., Ashouri A.R., Farmer L., and Saadat S.S. *Metallogeny of Mashhad Paleo-Tethys Granitoids, NE Iran*. Millpress, 1169-1173 pp. (2003).
11. Mirnejad H. Geochemistry and petrography of Mashhad granites and pegmatites. *M.Sc. Thesis*, Tehran University (1991).
12. Iranmanesh J. and Sethna S.F. Petrography and geochemistry of the Mesozoic granite at Mashhad, Khorasan Province, northeastern part of Iran. *Journal of the Geological Society of India*, **52**(1): 87-94 (1998).
13. Abbasi H. Petrology of regional and contact metamorphic rocks south of Mashhad. *M.Sc. Thesis*, Tehran University (1998).
14. Ghazi M., Hassanipak A.A., Tucker P.J., and Mobasher K. Geochemistry and 40Ar-39Ar ages of the Mashhad Ophiolite, NE Iran. abstracts as: Eos. Trans. AGU, **82**(47), Fall Meet. (2001).
15. Stampfli G.M. The Intra-Alpine terrain: a Paleo-Tethyan remnant in the Alpine Variscides. *Eclogae Geol. Helv.*, **89**(1): 13-42 (1996).
16. Stampfli G.M. Tethyan oceans. In: Bozkurt E., Winchester J.A., and Piper J.D.A. (Eds.), *Tectonics and Magmatism in Turkey and Surrounding Area*. Geological

Society of London, Special Publication 173, 163-185 pp. (2000).
17. Stampfli G.M. Opening and closure of Paleo-Tethys in Iran. Personal communication (2002).
18. Stampfli G.M. and Pillevuit A. An alternative Permo-Triassic reconstruction of the kinematics of the Tethyan realm. In: Dercourt J., Ricou L.-E., and Vrielinck B. (Eds.), *Atlas Tethys Palaeoenvironmental Maps, Explanatory Notes*. Gauthier-Villars, Paris, 55-62 pp. (1993).
19. Stampfli G.M., Marcoux J., and Baud A. Tethyan margins in space and time. In: Channell J.E.T., Winterer E.L., and Jansa L.F. (Eds.), *Paleogeography and Paleoceanography of Tethys*. Palaeogeography, Palaeoclimatology, Palaeoecology, 87, 373-410 pp. (1991).
20. Davoudzadeh M., and Schmidt K. Plate tectonics, orogeny, and mineralization in the Iranian fold belts; report of a German-Iranian research program 1977-19. Neues Jahrbuch fuer Geologie und Palaeontologie. *Abhandlungen*, **168**(2-3): 182-207 (1984).
21. Stocklin J. Possible ancient continental margins in Iran. In: Burk C.A. and Drake C.L. (Eds.), *The Geology of Continental Margins*. 873-887 pp. (1974).
22. Ruttner A.W. The Pre-Liassic Basement of the Eastern Kopet Dogh ranges. *N. Jb. Geol. Palaont Abh*, **168**(2/3): 236-265 (1984).
23. Baud, A. and Stampfli G.M. Tectonogenesis and evolution of the Cimmerides: the volcanic-sedimentary Triassic of Aghdarband (Kopet-Dagh, North-East Iran). In: Sengor A.M.C. (Ed.), *Tectonic Evolution of the Tethyan Region*. 265-275 pp. (1989).
24. Kunin, N. *et al.*, Map of depth to Moho, Moscow: Institute of Physics of the Earth (1987).
25. Majidi B. The ultrabasic lava flows of Mashhad, North East Iran. *Geological Magazine*, **118**(1): 49-58 (1981).
26. Eftekharnezhad J. and Behroozi A. Geodynamic and significance of recent discoveries of ophiolite and Late Paleozoic rocks in Ne Iran (including Kopet Dogh): Geological Survey of Iran, internal report, p. 21 (1989).
27. Khatonie Molayossefi M., The study of stratigraphy and plants fossils of Shemshak formation in Shandiz area. *M.Sc. Thesis*, p. 222 (2000).
28. Hall S. and Sturrock V. Tectonic Control on the Creation of Supergiant Fields in the Central and South Caspian Area. *The Bulletin, Houston Geological Society*, **43**(5): 12-15 (2001).
29. Robinson P., Higgins N.C., and Jenner G. Determination of rare-earth elements, Yttrium and Scandium in rocks by using an ion exchange-X-Ray Fluorescence technique. *Chemical Geology*, **55**: 121-137 (1986).
30. Nachit H., Razafimahefa N., Stussi J.M., and Carron J.P. Composition chimique des biotites et typologie magmatique des granitoïdes. *C.R. Acad. Sci.*, Paris, **301**: 813–818 (1985).
31. Leaked B.E., Woolley A.R., Arps C.E.S., Birch W.D., Gilbert M.C., Grice J.D., *et al.* Nomenclature of amphiboles: report of the subcommittee on amphiboles of the International Mineralogical Association commission on new minerals and mineral names. *Mineralogical-Magazine*, **61**(2): 295-321 (1997).
32. Schmidt M.W. Amphibole composition in tonalite as a function of pressure: an experimental calibration of the Al-hornblende barometer. *Contribution to Mineralogy and Petrology*, **130**: 304-310 (1992).
33. Frost B.R., Barnes C.G., Collins W.J., Arculus R.J., Ellis D.J., and Frost C. A Geochemical Classification for Granitic Rocks. *Journal of Petrology*, **42**: 2033-2048 (2001).
34. Rickwood P.C. Boundary lines within petrologic diagrams which use oxides of major and minor elements. *Lithos*, **22**: 247-267 (1989).
35. Whalen J.B., Currie K.L., and Chappell B.W. A-type granites. geochemical characteristics, discrimination and petrogenesis. *Contributions to Mineralogy and Petrology*, **95**: 407-419 (1987).
36. Barbarin B. A review of the relationships between granitoid types, their origin and their geodynamic environments. *Lithos*, **46**: 605-626 (1999).
37. Villaseca C., Barbero L., and Herreros V. A re-examination of the typology of peraluminous granite types in intra continental orogenic belts. *Transaction of the Royal Society of Edinburgh; Earth Sciences*, **89**: 113-119 (1998).
38. Debon F., and Le Fort P. A chemical-mineralogical classification of common plutonic rocks and associations. *Ibid.*, **73**: 135-49 (1983).
39. Ishihara S. The magnetite-series and ilmenite-series granitic Rocks. *Mining Geology*, **27**: 293-305 (1977).
40. Barker F. Trondhjemite: definition, environment and hypotheses or origin. In: Barker F. (Ed.), *Trondhjemites, Dacites, and Related Rocks*. 1-12 pp., Elsevier, New York (1979).
41. Pearce J.A., Harris N.B.W., and Tindle A.G. Trace element discrimination diagrams for the tectonic interpretation of granitic rocks. *Journal of Petrology*, **25** (4): 956-983 (1984).